Asian Journal of Physics
Vol. 30, No 6 (2021) 863-870
Available on: www.asianjournalofphysics.com

ap

Higher order photonic stop-bands and random lasing in microflower decorated polystyrene opals

N N Subhashree Ojha[1], Anirban Sarkar[1,2], and B N Shivakiran Bhaktha[1,*]

[1]*Department of Physics, Indian Institute of Technology Kharagpur, Kharagpur-721 302, India*

[2]*Advanced Technology Institute, Department of Electrical and Electronic Engineering, University of Surrey, Guildford, GU2 7XH, United Kingdom*

Dedicated to Professor D N Rao for his significant contributions and pioneering works in the fields of spectroscopy, optics, nonlinear optics and photonics

Mono-sized polystyrene nanoparticles of different diameters were synthesized using emulsion polymerization process. Consequently, highly ordered 3-D photonic crystals (opals) of polystyrene nanoparticles were fabricated by evaporation assisted sedimentation deposition technique. The opal structures were found to exhibit very intense higher order photonic stop-bands (PSBs) along with the fundamental PSB. Numerically computed band diagram of polystyrene opal endorses the higher order energy bands in the experimental reflection spectra and the existence of Van Hove singularity. Also, on coating the opal structure with a 4-(dicyanomethylene)-2-methyl-6-(4-dimethylaminostyryl)-4H-pyran (DCM) doped polyvinyl alcohol (PVA) thin film (DCM-PVA) active layer, random lasing (RL) was observed.

Keywords: 3-D photonic crystal, Polystyrene microflower, Higher order photonic stop-bands, Van Hove singularity, Random laser.

1 Introduction

Photonic crystals (PCs) are a special class of periodic optical structures that affect the motion of photons likewise the atomic lattice does for electrons in an atomic crystal. Periodic modulation in the electric permittivity of PCs give rise to photonic stop-bands (PSBs) which prohibits the propagation of photons with energies within the band in certain directions [1-3]. Depending on the dimensionality of the periodicity of dielectric constant, PCs are classified into one-dimensional (1-D), two-dimensional (2-D) and three-dimensional (3-D) PCs [4]. According to modified Bragg's law the periodicity of these optical super lattice structures is required to be comparable with the wavelength of light. Therefore, fabrication of a PC with PSB in the visible or near infrared wavelength region is quite challenging, and can lead to a wide range of applications in optoelectronics such as waveguides [5], low threshold lasers [6], optical sensors [7], optical filters [8,9] and switches [10,11].

Possession of PSB in all the three directions distinguishes 3-D PCs from the other two classes wherein complete confinement of photons is not possible. Opals are artificially fabricated 3-D PCs comprising of monosized nanoparticles [12-15]. Relatively simple and inexpensive fabrication technique based on the self-assembly of monodispersed nanoparticles in a colloidal solution highlights the advantage of studying the optical properties of opals. Although opals have modulation of dielectric constant along three dimensions, the

Corresponding author
e mail: kiranbhaktha@phy.iitkgp.ac.in (B N Shivakiran Bhaktha)
doi: https://doi.org/10.54955/AJP.30.6.2021.863-870

weak contrast in dielectric constant with the background results in pseudo photonic band-gap (PBG) instead of a complete PBG. In spite of this shortcoming, in recent times, there has been increased interest in opals, primarily silica and polystyrene (PS) opals, because of their ability to confine, manipulate and control light [16,17]. PS opals have some specific advantages over silica opals because of their higher refractive index and lower melting temperature compared to silica. Furthermore, the features in the high energy stop-bands of the PCs [18-20] are interesting because of their low dispersion properties and low group velocity, owing to the increased flatness of the bands. Consequently, the incident waves interact strongly with the PC at the higher order band edges, which eventually increases the probability of the nonlinear optical phenomena.

In order to observe the high energy stop-bands for the opals, their crystalline nature is of great importance. In this regard, synthesis of monodispersed nanoparticles and the opal growth techniques are of major concern that need to be carefully monitored and controlled. Furthermore, the growth of the composite materials composed of randomly distributed nanostructures in a photonic crystal are of great interest to researchers working on random lasers [21] and disordered systems. In a random laser, multiple scattering of light can provide sufficient feedback to amplify the light emitted by an active medium without requiring any feedback mirror. Therefore, due to absence of any well-defined cavity, lasing modes are randomly distributed over the gain spectrum. In this work, we report on the fabrication of highly crystalline PS opals of different lattice constants decorated with PS microflowers. Alongside the random distribution of the microflowers on the PC, evidence of nanoribbons wrapping the nanoparticles makes this system a hybrid structure. Highly crystalline arrangement of the PS nanoparticles obtained by the self-assembly technique exhibits higher order PSB and Van Hove singularity [19]. Numerically computed band diagram of the PS opal endorses the existence of the higher order stop-band and Van Hove singularity peaks in the experimentally obtained reflection spectra. Furthermore, random lasing properties of the DCM-PVA coated opal structure has been investigated, wherein the higher order PSB overlaps with the gain spectrum of the DCM-PVA thin film.

2 Fabrication details, Result and Discussion

2.1 Polystyrene nanoparticles and microflowers synthesis

Monodispersed PS nanoparticles were synthesized by emulsion polymerization technique [22] using potassium persulfate (Sigma Aldrich) as initiator, sodium lauryl sulfate (Vetec) as emulsifier, and aqueous alcohol (mixture of deionized water (DIW) and ethanol) as dispersing medium. Quantitative amount of potassium persulfate (0.054 g) and sodium lauryl sulfate (0.055 g) were dissolved in 70 ml of ethanol-DIW (5:2 volume ratio) solution in a 250 ml 3 neck flask. To remove the anti-polymerizing agent, styrene was washed with 10 % sodium hydroxide solution in a separate funnel four times. Then certain amount of styrene was added under nitrogen atmosphere. The emulsion solution was heated at 90 ºC under rapid stirring for 8 hours. After the polymerization reaction, in order to remove the oligomers, the solution was filtered with glass wools and then centrifuged (REMI RM-12C) four times at 5000 rpm for 30 minutes and washed in DIW. During the centrifugation process the nanoribbons responsible for the formation of microflowers were observed floating on the supernatant liquid due to their lower densities with respect to the PS spheres. During the removal of DIW after washing the nanoparticles, the floating nanoribbons were preserved very cautiously inside the centrifuge tube. Finally, the PS nanoparticles and nanoribbons were dried to make them free of solvent. PS nanoparticles of three different sizes (PS1, PS2, and PS3) were synthesized using styrene volume of 2.25 ml, 2 ml, and 1.75 ml, respectively.

2.2 Fabrication and characterization of polystyrene opals

PS microflowers decorated opals were fabricated using evaporation assisted sedimentation deposition (EASD) technique [23]. This technique is based on the convective self-assembly of colloids on a glass substrate by the action of moving meniscus. Firstly, the substrates were cleaned with acetone and ethanol. Then, they were kept in 3 ml vials each containing aqueous solutions of PS nanoribbons and nanoparticles

of a particular size. The substrates were inclined at 75º angle with respect to the base of the vials. The vials were then kept inside a temperature-controlled oven at 40 °C. As the effective density of the dispersed nanoparticles is lower than the density of water, PS particles easily float on the surface of water leading to its slower evaporation. The evaporation of water slowly lowers the level of meniscus, sticking the PS nanoparticles on the substrate in a close packed manner.

The PS nanoparticle size depends on several parameters such as initiator, monomer, temperature, and duration of the reaction. By changing the styrene (monomer) volume, we were able to obtain the PS particles of different sizes. The scanning electron microscope (SEM) images were used to measure the particle size to confirm the homogeneous size distribution and the face centered cubic (FCC) stacking of the particles. An opal fabricated in FCC structure using PS nanoparticles PS1 has been shown in Fig 1(a) along with an embedded microflower. SEM images of the PS2 and PS3 opals have also been shown in Fig 1(b) and Fig 1(c), respectively. PS nanoparticles PS1, PS2 and PS3 were observed to have diameters of 586 ± 19 nm, 480 ± 13 nm, and 400 ± 17 nm, respectively from the SEM images, and are tabulated in Table 1. Figure 1(d) shows multiple microflowers distributed over a larger area of the opal structure, while nanoribbons wrapping PS nanoparticles have been shown in Fig 1(e). As the PS nanoribbons are less denser than the PS nanoparticles, the nanoribbons float at the top of the aqueous suspension during EASD. Hence, the upper region of the deposited opal film alone hosts the microflowers. Moreover, the nanoribbons wrapping the PS nanoparticles not only appeared on the surface of the film, but they were also present deep inside the bulk crystal.

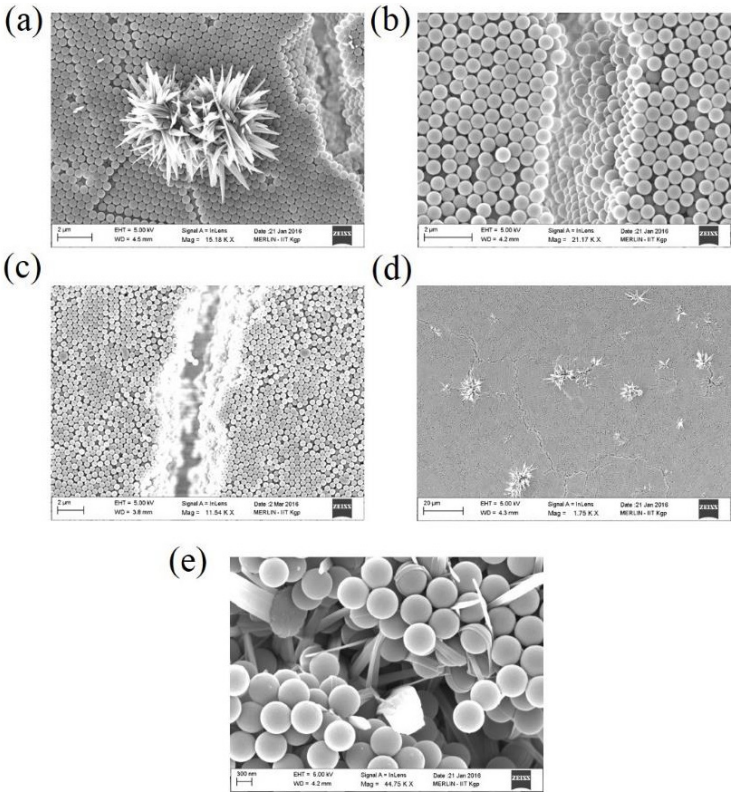

Fig 1. SEM images of the opals: (a) PS1 along with a microflower, (b) PS2 and (c) PS3. (d) Larger area image of PS3 opal with multiple microflower structures distributed on the surface and (e) the nanoribbons wrapping the nanoparticles.

The reflection spectra of the opals fabricated using PS1, PS2, and PS3 PS nanoparticles, were recorded using aluminium mirror as a reference with the help of a fiber coupled Avantes UV-Visible spectrometer having a spectral resolution of 0.4 nm, and are depicted in Fig 2. The reflection spectra show the fundamental PSB as well as the higher order PSBs which reveal the high-quality crystalline nature of the fabricated opals. Reflection from the PS opals follows the modified Bragg's law [24]:

$$m\lambda_{ps} = \sqrt{\frac{8}{3}} \cdot d \cdot (n_{eff}^2 - \sin^2\varphi)^{1/2} \tag{1}$$

where, m is the order of reflection peak, λ_{ps} the reflection peak wavelength, d is the diameter of the PS nanoparticle, n_{eff} is the effective refractive index of the system, and φ is the angle of incidence of light. Effective refractive index of the system is given by,

$$n_{eff} = \sqrt{f \cdot n_{ps}^2 + (1-f) \cdot n_{air}^2} \tag{2}$$

n_{ps} and n_{air} are the refractive indices of PS spheres and the background air respectively and f is the packing fraction of the PS spheres. In our system, we consider the refractive indices n_{ps} = 1.59, n_{air} = 1, and the packing fraction f = 0.74 due to the FCC crystalline nature of the PS opals that is evident from the SEM images in Fig 1.

Being highly crystalline in nature, all the three opal structures support higher order stop-bands along with the fundamental one. In the reflection spectrum of PS1 opal shown in Fig 2(a), the fundamental PSB appears at 1396 nm with reflectance value of 69%, which is due to the reflection of light from [111] lattice plane and the two peaks at 720 nm and 775 nm with the reflectance values of 14% and 16%, respectively correspond to the higher order stop-bands. Among these two higher order asymmetric peaks, the peak at 720 nm corresponds to the second order PSB due the [111] lattice planes and the other peak is attributed to the Van Hove singularity and is discussed later with the help of simulations. Similarly, the first order stop-band for PS2 opal occurs at 1137 nm with reflectance value of 50% and two peaks for the higher order stop-bands occur at 572 nm and 630 nm with 8% and 10% reflectivity values, respectively as illustrated in

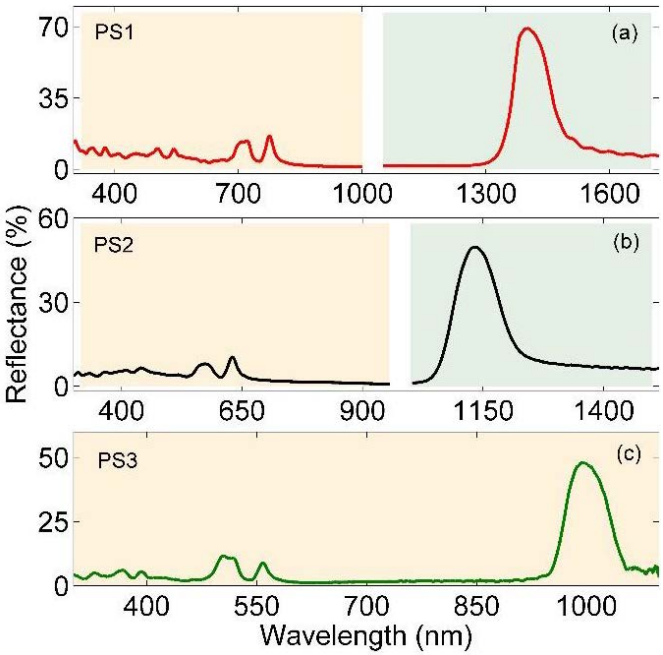

Fig 2. Reflection spectra of fabricated PS opals with monosized nanoparticles of different sizes: (a) PS1, (b) PS2 and (c) PS3.

Fig 2(b). In the case of PS3 opal as shown in Fig 2(c), the position of the first order PSB is at 993 nm with 48% reflectivity and that of higher order stop-bands are at 504 nm and 558 nm with the reflectivity values of 11% and 9%, respectively. It is evident that the PSB experiences a blue-shift for opals fabricated with smaller PS nanoparticles. In the reflection study, the diameter of the incident light beam was ~ 4 mm, which was larger than the size of the individual microflower and the domain of the opal structure. Hence, the reflected light collected from the structure exhibit an area-averaged reflection property of composite system. Moreover, the microflowers and nanoribbons were distributed only at upper region of the deposited film and also their number density was very less. Hence, no significant effect of the microflowers and nanoribbons on the reflection spectra of the PCs was observed. By utilizing the modified Bragg's law for reflection, lattice constants as well as the particle sizes of the opals were estimated from the experimental reflection peaks and compared with the SEM results and are presented in Table 1. The calculated value of the diameters of nanoparticles of the PS1, PS2, and PS3 opals from the reflection spectra are in good agreement with that obtained from SEM images. It is to be noted that the higher order energy bands are more vulnerable to the disorder present in the crystal than the first order band [25]. Therefore, the existence of the finite amount of disorder, though it is quite small, might be the reason for the non-Lorentzian line shape of the higher order reflection peaks.

Table 1. The volume of styrene used for the synthesis of PS nanoparticles of different sizes are presented. The particle sizes are measured by SEM and calculated using the stop-bands observed in the reflection spectra.

Polystyrene nanoparticles	Styrene volume	Particle size from SEM	Particle size from reflection spectrum
PS1	2.25 ml	586 ± 19 nm	579 nm
PS2	2.00 ml	480 ± 13 nm	472 nm
PS3	1.75 ml	400 ± 17 nm	417 nm

Photonic bands of the PS opals have been numerically simulated using MIT Photonic Band (MPB) software [26], taking the lattice constant of the PC as a unit of length. The simulated band diagram has been presented in Fig 3 along with the experimental reflection spectrum of PS3 opal. The appearance of PSBs in experimentally obtained reflection spectrum matches quite well with the simulated PSB positions. The first order PSB occurs around $a/\lambda = 0.6$ due to the reflection of light by the [111] lattice planes. The

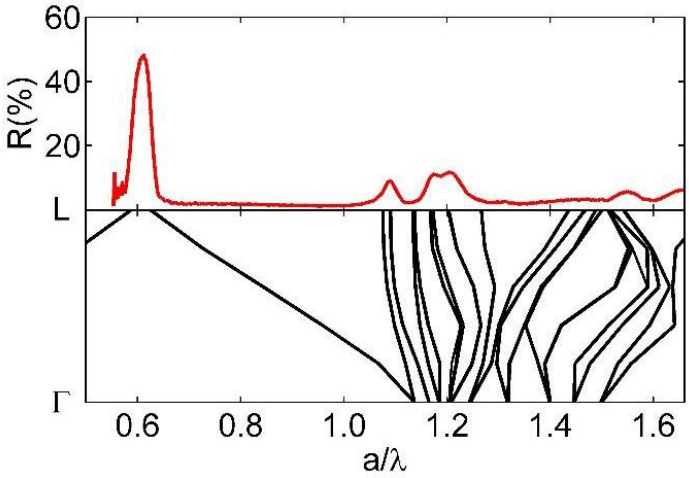

Fig 3. Reflection spectrum of PS3 opal at normal incidence (top) and the band structure along Γ-L direction (bottom).

higher order peak centered around $a/\lambda = 1.2$ represents the second order PSB due to the reflection of light by the [111] planes which appears at exactly half the wavelength value of the fundamental PSB position. Photonic bands having energies higher than the first order PSB correspond to the photon momentum which lies outside the first Brillouin zone and are folded back into the first Brillouin zone. These folded bands generally have nonlinear energy dispersion property and can have critical points such as maxima, minima, and saddle points. In three dimensions, the density of states attains a very high value due to the occurrence of a critical point which is known as Van Hove singularity. The Van Hove singularity is a saddle point in the band diagram with a large density of state value and moves to lower energies with increasing angle of incidence of light [19,20]. Therefore, the other higher order peak which appears around $a/\lambda = 1.1$ stands for the Van Hove singularity peak. The Van Hove singularity also signifies the excitation of photonic modes in the photonic crystal.

2.3 Random lasing in DCM-PVA coated opal

To study the random lasing properties, opal structure was coated with a DCM-PVA thin film which acted as the active medium. First, DCM and PVA were dissolved separately in a common solvent dimethyl sulfoxide (DMSO) with their respective concentrations at 2 mM and 250 mg/ml. The final solution was prepared by mixing these two solutions in 1:3 ratio. DCM-PVA solution was then coated on the opal structure by using spin coating technique and the film was dried at 60 ºC for 20 min. The structure was optically pumped by a nano-second laser (532 nm, 20 Hz, 10 ns) using a cylindrical lens of focal length 5 cm. In the emission of DCM-PVA coated opal structure, random lasing characteristics were observed. Typical pump energy dependent lasing threshold behavior of the emission was recorded and has been shown in Fig 4, wherein the slope efficiency of the emission changes above the random lasing threshold value of 0.28 mJ.

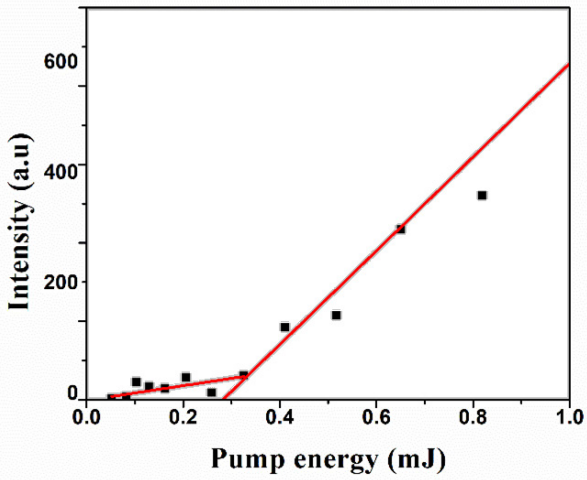

Fig 4. Output random lasing intensity vs input pump energy with the random lasing threshold at 0.28 mJ.

To investigate the lasing properties further, we carried out pump stripe length dependent emission study which has been plotted in Fig 5. We observed that the random lasing modes change due to pumping the system with different pump stripe lengths that confirmed the RL emission from the structure. Origin of the random lasing from the structure can be attributed to light scattering mediated feedback provided by the microflowers and that by the density fluctuations inside the film. However, major contribution in the light scattering should be from the microflowers due to their large sizes. Also, emission of the DCM-PVA film coincides with the second order photonic band gap of the opal structure which provides additional feedback to further reduce the lasing threshold.

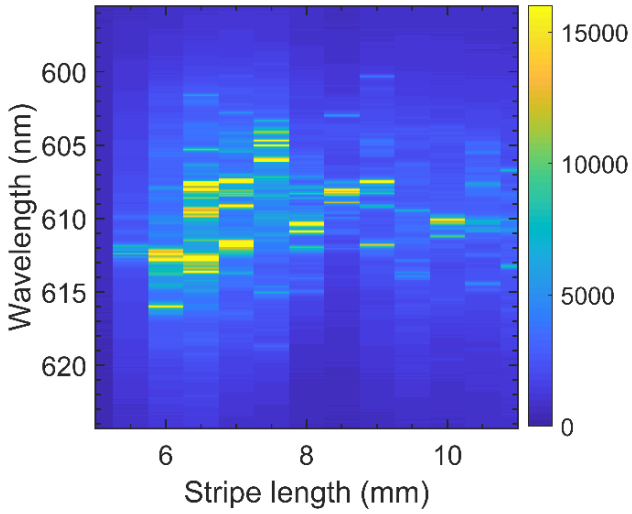

Fig 5. Stripe length dependent random laser emission spectra showing change of the random lasing modes.

3 Conclusion

Polystyrene monodispersed nanoparticles and nanoribbons were synthesized by emulsion polymerization technique. Nanoparticles of three different diameters (PS1, PS2, and PS3) were obtained by varying the styrene volume as 2.25ml, 2ml, and 1.75ml, respectively. Synthesized nanoparticles were self-assembled by EASD method to fabricate microflowers decorated opals. SEM images show the monodispersity of the nanoparticles and the formation of the microflower structure. All the three PS opals, PS1, PS2, and PS3 support two higher energy peaks along with the fundamental PSB peak for [111] planes due to their extremely high crystalline nature in the reflection spectra. The high energy reflection peaks have been analyzed with the help of simulated photonic band diagram of PS opal. One of them with comparably higher energies is attributed to the second order peak for [111] planes, which appears exactly at the energy value double of the first order PSB and the other is attributed to the Van Hove singularity of the crystal, which stands for the coupling of the incident light with the photonic modes of the polystyrene opals. Random lasing behavior of the DCM-PVA coated opal structure was investigated. Light scattering by the microflowers and the density fluctuations inside the film contributed to the optical feedback to obtain laser oscillations and generated randomly distributed lasing modes in the emission. It was also observed that the second order photonic band gap of the opal structure helps in further reducing the random lasing threshold.

References

1. John S, Strong Localization of Photons in Certain Disordered Dielectric Superlattices, *Phys Rev Lett*, 58(1987)2486–2489.
2. Yablonovitch E, Inhibited Spontaneous Emission in Solid-State Physics and Electronics, *Phys Rev Lett*, 58(1987)2059–2062.
3. Joannopoulos J D, Villeneuve P R, Fan S, Photonic crystals: putting a new twist on light, *Nature*, 386(1997)143–149.
4. Joannopoulos J D, Johnson S G, Winn J N, Meade R D, Photonic crystals Molding the Flow of Light, 2nd edn, (Princeton University Press, NJ), 2008.
5. Lončar M, Doll T, Vučković J, Scherer A, Design and Fabrication of Silicon Photonic Crystal Optical Waveguides, *J Lightwave Technol*, 18(2000)1402–1411.
6. Painter O, Lee R K, Scherer A, Yariv A, O′Brien J D, Dapkus P D, Kim I, Two-Dimensional Photonic Band-Gap Defect Mode Laser, *Science*, 284(1999)1819–1821.

7. Nair R V, Vijaya R, *Photonic crystal sensors: An overview, Progress in Quantum Electronics*, 34(2010)89–134.
8. Costa R, Melloni A, Martinelli M, Bandpass Resonant Filters in Photonic-Crystal Waveguides, *IEEE Photonics Technol Lett*, 15(2003)401–403.
9. Koirala1 I, Shrestha V R, Park C-S, Lee S-S, Choi D-Y, Polarization-Controlled Broad Color Palette Based on an Ultrathin One-Dimensional Resonant Grating Structure, *Sci Rep*, 7(2017)40073; doi. doi.org/10.1038/srep40073.
10. Tanabe T, Notomi M, Mitsugi S, Shinya A, Kuramochi E, All-optical switches on a silicon chip realized using photonic crystal nanocavities, *Appl Phys Lett*, 87(2005)151112; doi.org/10.1063/1.2089185.
11. Bingi J, Nair R V, Vijayan C, Time dependent Bloch mode transmittance in self-assembled random photonic crystal for photonic time delay switching, *Opt Mater*, 64(2017)95–99.
12. Vlasov Y A, Bo X-Z, Sturm J C, Norris D J, On-chip natural assembly of silicon Photonic bandgap crystals, *Nature*, 414(2001)289–293.
13. Blanco A, Chomski E, Grabtchak S, Ibisate M, John S, Leonard S W, Lopez C, Meseguer F, Miguez H, Mondia J P, Ozin G A, Toader O, Driel H M V, Large-scale synthesis of a silicon photonic crystal with a complete three-dimensional bandgap near 1.5micrometres, *Nature*, 405(2000)437–440.
14. Meng Y, Tang B, Ju B, Wu S, Zhang S, Multiple Colors Output on Voile through 3D Colloidal Crystals with Robust Mechanical Properties, *ACS Appl Mater Interfaces*, 9(2017)3024−3029.
15. Li F, Tang B, Wu S, Zhang S, Facile Synthesis of Monodispersed Polysulfide Spheres for Building Structural Colors with High Color Visibility and Broad Viewing Angle, *Small*, 13(2017)1602565; doi.org/10.1002/smll.201602565.
16. Colvin V L, From Opals to Optics: Colloidal Photonic Crystals, *MRS Bull*, 26(2011)637–641.
17. Lodahl P, Driel A F V, Nikolaev I S, Irman A, Overgaag K, Vanmaekelbergh D, Vos W L, Controlling the dynamics of spontaneous emission from quantum dots by photonic crystals, *Nature*, 430(2004)654–657.
18. García-Santamaría F, Galisteo-López J F, Braun P V, López C, Optical diffraction and high-energy features in three-dimensional photonic crystals, *Phys Rev B*, 71(2005)195112; doi.org/10.1103/PhysRevB.71.195112.
19. Pavarini E, Andreani L C, Soci C, Galli M, Marabelli F, Comoretto D, Band structure and optical properties of opal photonic crystals, *Phys. Rev. B* 72(2005)045102; doi.org/10.1103/PhysRevB.72.045102.
20. Nair R V, Vijaya R, Observation of higher-order diffraction features in self-assembled photonic crystals, *Phys Rev A*, 76(2007)053805; doi.org/10.1103/PhysRevA.76.053805.
21. Dominguez C T, Lacroute Y, Chaumont D, Sacilotti M, de Araújo C B, Gomes A S L, Microchip Random Laser based on a disordered TiO2-nanomembranes arrangement, *Opt Express*, 20(2012)17380–17385.
22. Alee K S, Sriram G, Rao D N, Spectral and morphological changes of 3D polystyrene photonic crystals with the incorporation of alcohols, *Opt Mater*, 34(2012)1077–1081.
23. Chiappini A, Armellini C, Chiasera A, Ferrari M, Jestin Y, Mattarelli M, Montagna M, Moser E, Conti G N, Pelli S, Righini G C, Gonçalves M C, Almeida R M, Design of photonic structures by sol–gel-derived silica nanospheres, *J Non Cryst Solids*, 353(2007)674–678.
24. Reculusa S, Ravaine S, Synthesis of Colloidal Crystals of Controllable Thickness through the Langmuir-Blodgett Technique, *Chem Mater*, 15(2003)598–605.
25. Soukoulis C M, Photonic Crystals and Light Localization in the 21st Century, (Springer Science + Business Media, Dordrecht), 2001.
26. Johnson S G, Joannopoulos J D, Block-iterative frequency-domain methods for Maxwell's equations in a planewave basis, *Opt Express*, 8(2001)173–190.

[*Received*: 03.03.2021; *accepted*: 09.05.2021]